BJR

BONE FRACTURE

MicroRNA-186 improves fracture healing through activating the bone morphogenetic protein signalling pathway by inhibiting SMAD6 in a mouse model of femoral fracture

AN ANIMAL STUDY

C. Wang,
G-F. Zheng,
X-F. Xu

Fudan University Shanghai Cancer Center, Shanghai, China

Objectives

MicroRNAs (miRNAs) have been reported as key regulators of bone formation, signalling, and repair. Fracture healing is a proliferative physiological process where the body facilitates the repair of a bone fracture. The aim of our study was to explore the effects of microRNA-186 (miR-186) on fracture healing through the bone morphogenetic protein (BMP) signalling pathway by binding to Smad family member 6 (SMAD6) in a mouse model of femoral fracture.

Methods

Microarray analysis was adopted to identify the regulatory miR of SMAD6. 3D micro-CT was performed to assess the bone volume (BV), bone volume fraction (BVF, BV/TV), and bone mineral density (BMD), followed by a biomechanical test for maximum load, maximum radial degrees, elastic radial degrees, and rigidity of the femur. The positive expression of SMAD6 in fracture tissues was measured. Moreover, the miR-186 level, messenger RNA (mRNA) level, and protein levels of SMAD6, BMP-2, and BMP-7 were examined.

Results

MicroRNA-186 was predicted to regulate SMAD6. Furthermore, SMAD6 was verified as a target gene of miR-186. Overexpressed miR-186 and SMAD6 silencing resulted in increased callus formation, BMD and BV/TV, as well as maximum load, maximum radial degrees, elastic radial degrees, and rigidity of the femur. In addition, the mRNA and protein levels of SMAD6 were decreased, while BMP-2 and BMP-7 levels were elevated in response to upregulated miR-186 and SMAD6 silencing.

Conclusion

In conclusion, the study indicated that miR-186 could activate the BMP signalling pathway to promote fracture healing by inhibiting SMAD6 in a mouse model of femoral fracture.

Cite this article: *Bone Joint Res* 2019;8:550–562.

Keywords: MicroRNA-186, SMAD family member 6, Fracture healing, BMP signalling pathway, Femoral fracture

Article focus

- Optimal therapeutic and prognostic biomarkers that indicate bone healing process have not been clearly identified.
- We explored the effects of microRNA-186 (miR-186) on bone healing in a mouse model of femoral fracture.

Key messages

- Upregulation of miR-186 could promote fracture healing in mice with femoral fracture.
- Upregulated miR-186 and inhibited SMAD family member 6 (SMAD6) could elevate bone mineral density (BMD) and bone volume fraction (BV/TV), and could promote callus formation.
- Upregulated miR-186 activates the bone morphogenetic protein (BMP) signalling pathway via inhibition of SMAD6.

Strengths and limitations

- We characterized the molecular mechanism of miR-186 in improving fracture

Correspondence should be sent to X-F. Xu; email: xuxiaofeng@live.cn

doi: 10.1302/2046-3758.811.BJR-2018-0251.R1

Bone Joint Res 2019;8:550–562.

healing via the BMP signalling pathway by binding to SMAD6.

- We used 3D micro-CT and a biomechanical test to validate the effect of miR-186 on bone healing.
- The expression patterns of miR-186 were not identified in other phases of bone healing.

Introduction

Fracture healing is complex due to a number of factors including the interaction between cells, molecules, and biological pathways.[1] Healing begins with an initial inflammatory response, during which time the immune system and the bone interact intimately, and is then followed by a regenerative phase.[2] A delay in fracture healing poses a significant clinical and economic burden for patients and health services.[3] Furthermore, the biology of fracture healing is characterized by a series of complicated biological processes that possess particular regenerative patterns and differ in the expression of several thousand genes.[4] The current and most commonly used method of monitoring the therapeutic response of patients and those at high risk is through the measurement of bone mineral density (BMD).[5] In addition, stress fracture healing can also be used, which is depicted by the remodelling that progresses in both the fracture line and woven bone, proliferating at the sites of the fracture.[6] Recently, evidence has been produced which has shown that microRNAs (miRNAs) modulate osteoblast, chondrocyte, and osteoclast differentiation, along with function. This suggests that miRNAs can act as key regulators of resorption, remodelling, and bone formation, as well as repair.[7]

miRNAs are small non-coding RNAs that have been found to have an effect in gene expression.[8] There have been a number of studies suggesting that miRNAs play vital roles in osteogenesis and skeletal homeostasis and recently Sun et al[9] have demonstrated the regulatory function of miR-21 in osteogenesis *in vitro*. A previous microarray analysis identified the function of various types of miRNAs and showed that the alteration of expression patterns may exert critical effects on the pathogenesis of impaired fracture healing.[10] Li et al[11] have also highlighted the high expression of miR-214-5p found in the plasma of patients with a hand fracture or intra-articular calcaneal fracture and demonstrated the importance of downregulation of miR-214-5p that resulted in the enhancement of osteoblastic cell viability and resistance to apoptosis. MicroRNA-186 was first discovered in human osteoblast sarcoma cell line Saos-2, and also in mouse eye tissue, which is located in intron 8 of the precursor messenger RNA (mRNA) of the zinc finger protein 265.[12] The involvement of miR-186 and its regulatory effect has been discovered in pancreatic islet-like cell clusters differentiated from human embryonic stem cells[13] and also in patients suffering from cardiovascular disease.[14] Furthermore, downregulation in miR-186 was observed in various tumour cells, manifesting tumour-suppressing properties.[15] An example of this is in the significant decrease in the expression of miR-186 that was observed in non-small cell lung cancer and overexpression of miR-186 that was also found to significantly inhibit the proliferation, migration and invasion of non-small cell lung cancer cells.[16] The expression of miR-186 was also observed to be upregulated in tumours showing proto-oncogene activity. The upregulation of miR-186 expression in pancreatic ductal adenocarcinoma, which is particularly elevated in patients with large tumours, lymph node metastasis, and short survival are examples of the proto-oncogenic properties of miR-186.[17]

The overexpression of miR-186 has been reported to target and inhibit SMAD family member 6 (SMAD6).[18] The preliminary *in silico* prediction indicated that miR-186 was a regulatory miR of SMAD6 related to fracture healing. Although it is known that SMAD6 is a critical feedback inhibitory governor of bone morphogenetic protein (BMP)/SMAD signalling, there is very little known on the post-transcriptional modification of inhibitory SMADs and the mechanisms through which their roles are adjusted.[19] The BMP signalling pathway can also modulate a number of pathways that are involved in endochondral bone formation.[20] However, few studies have clarified the correlation between miR-186, SMAD6, and fracture healing. This study was conducted in order to explore the influences of miR-186 on fracture healing by targeting SMAD6 through the BMP signalling pathway in the mouse model of femoral fracture.

Materials and Methods

Microarray analysis. Activation of the BMP signalling pathway is critical for fracture healing,[21,22] and SMAD6 has an inhibitory effect on the BMP signalling pathway.[23] However, the exact role played by SMAD6 in bone fracture remains unclear. Therefore, four databases (microRNA.org, TargetScan, starBase, and DIANA) were searched to predict regulatory miRNAs in order to explore the molecular mechanisms of SMAD6. The predicted results were analyzed using the online analysis tool Venn (VIB/UGent, Gent, Belgium) to calculate and draw Venn diagrams.

Study subjects. Healthy male C57/BL mice of clean grade (six weeks old) were fed for two weeks in the mouse room of the laboratory. The mice were provided with conventional feeding and drinking in cages at room temperature (25°C). Afterwards, a total of 105 healthy male mice with a mean weight of 28.22 g (SD 2.50) were selected for the subsequent experiments. The mice were anaesthetized via an intraperitoneal injection of 2% sodium phenobarbital (30 mg/kg), with their knees flexed to 90° in the supine position. A median longitudinal incision of 1 cm was made over the patella of the right knee joint. An incision was also made on the medial margin of the patella of

the mice four biceps tendon and the joint capsule, for full exposure of the intercondylar sulcus of femur and patella. A stainless steel needle was inserted into the bone marrow to fix the level of the intertrochanteric fossa in femur. After cutting the handle of the steel needle, the needle tail was buried in the intercondylar fossa of the femur and the wound was closed, making sure the activity of the knee joint was not yet affected. The mice were then moved to a table and the lateral femur was fractured using a 200 g counterweight from a height of about 17 cm to 20 cm, with the counterweight adjusted according to the weight of the mouse. A radiation detecting system (Faxitron MX 20 X-Ray; Faxitron X-Ray Corporation, Wheeling, Illinois) was applied to detect the fracture condition and to assess the correct formation of the mouse model of femoral fracture. Having successfully established the fracture model, the mice then continued to be regularly fed and supplied with water in cages at room temperature.

Experimental mice treatment and grouping. The mice models were selected for further experiments, after which the following procedures were conducted: 12.5 μg of nucleic acid was diluted by the proper amount of pure water without endotoxin to 0.5 μg/μl, followed by the addition of 25 μl of 10% glucose solution (weight/volume (w/v)) to make the final glucose concentration reach 5% and the final volume reach 50 μl, after which it was fully mixed. Next, 25 μl of Entranster *in vivo* reagent (Engreen Biosystem Co., Ltd., Beijing, China) was diluted by 25 μl of 10% glucose solution, making the solution with 5% final glucose concentration and 50 μl of final volume, followed by full mixture. In addition, the diluted transfection reagent was added into diluted nucleic acid solution (Invitrogen Inc., Carlsbad, California), followed by full oscillation mixing and set at room temperature for 15 minutes. The mice were then anaesthetized through an intraperitoneal injection of 1% pentobarbital sodium (Beijing Chemical Reagents Company, Beijing, China) with a ratio of 0.5 mg/kg. Once the anaesthesia was administered, the operation site was disinfected by iodophor, injected 20 μl in total away from the fracture, and then the mice, after labelling, were observed in their cages. The mice were assigned to six groups (n = 15 for each group): a model group (without any treatment), a negative control (NC) group (continuously injected with 0.5 ml of normal saline via tail vein), a small interfering RNA (siRNA)-SMAD6 group (continuously injected with 200 μl of siRNA-SMAD6 solution via tail vein), a miR-186 mimic group (continuously injected with 200 μl of miR-186 mimic solution via tail vein), a miR-186 inhibitor group (continuously injected with 200 μl of miR-186 inhibitor solution via tail vein), and a miR-186 inhibitor + siRNA-SMAD6 group (continuously injected with 200 μl of miR-186 inhibitor solution and siRNA-SMAD6 solution via tail vein). The success rate of postoperative modelling was 85.71% (90/105).

Dual luciferase reporter gene assay. Dual luciferase reporter gene assay was used to detect whether SMAD6 was the direct target gene of miR-186. The full-length of the 3'-untranslated region (UTR) region in SMAD6 gene was cloned and amplified. Polymerase chain reaction (PCR) products were cloned into multiple sites of luciferase reverse primer of pmirGLO Dual-Luciferase miRNA Target Expression Vector (E1330; Promega Corporation, Madison, Wisconsin). Following this, the bioinformatics software was used to predict the site-directed mutagenesis of miR-186 and target gene binding sites and constructed the wild plants containing SMAD6 3'-UTR with miR-186 target site, which was named SMAD6-wild-type (Wt). Afterwards, the SMAD6 3'-UTR and miR-186 complementary sites were mutated, and the luciferase plasmid containing S mutant sequences was constructed, named as SMAD6-Mutant (Mut). The pRL-TK carrier (E2241; Takara Biotechnology Ltd., Liaoning, China) with expression of Renilla luciferase was regarded as the internal reference and was used to adjust the difference of transfection efficiency and cell number. The mice from the miR-186 and NC groups were respectively transfected into cells of fracture tissue. The dual luciferase activity assay was used in accordance with the method provided by Promega Corporation.

3D micro-computed tomography (3D micro-CT). A total of 15 femur specimens, five specimens from each group, were selected at 14, 28, and 42 days, respectively, followed by scanning with the use of the 3D micro-CT (uCT80; Scanco Holding AG, Wangen-Brüttisellen, Switzerland) with the conditions listed as follows: 27 μm of set scanning resolution, 450 mA of sweep current, 80 kV of sweep voltage, 20.5896 × 20.5896 × 20.5896 μm of position resolution, and 88 minutes of single scan-time. Afterwards, the standard phantom scan results equipped in random were collimated according to the requirements of the procedures set, and the 3D callus area region of interest (ROI) was re-established with femoral fracture end as the centre (5 mm × 5 mm × 6 mm), and the actual callus area was then measured through the manual selection of the callus area ROI in each of the ten scanning layers with the same length of 6 mm callus area among 300 scanning layers. Moreover, the data in newborn bone was obtained by subtracting the data in from the original bone of femur. Threshold distribution within femur bone was calculated with 1500 HU as the prevalue, including the bone volume (BV), the bone volume fraction (BVF, BV/TV), and BMD with image processing software (GE MicroView 2.1). Finally, the statistical analysis was conducted for data analysis.

Haematoxylin and eosin (H&E) staining and Masson's trichrome staining. The femur specimens were collected at 14, 28, and 42 days from mouse models after scanning by micro-CT and were fixed by 10% neutral formaldehyde for 48 hours. The femora were then decalcified

with 10% ethylenediaminetetraacetic acid (EDTA; ZSGB Biotechnology Inc., Beijing, China) for two weeks, with the solution being changed every three to five days. The specimens were embedded in paraffin and labelled. The specimens were frozen at least 20 minutes after the paraffin solidification and were cut into bone tissue sections with 5 μM of thickness continuously, followed by baking in sections overnight in order to prepare the tissue specimens. The tissue sections (5 μM) were routinely dewaxed and hydrated by H&E staining, rinsed by distilled water twice (two minutes per time), stained by haematoxylin for three minutes, and rinsed by running water for colour elimination. Afterwards, the specimens were placed in 1% hydrochloric acid ethanol solution for three to five seconds and rinsed by running water to retain blue staining. The specimens were stained by eosin for five minutes, conventionally dehydrated by gradient alcohol and mounted by neutral balsam. After Masson's trichrome staining, paraffin dewaxing, and hydration, the specimens were stained again with the use of Masson's trichrome dye (the proportional mixture of Weigert's iron haematoxylin A, B solution) for five minutes, rinsed with tap water, differentiated with 1% hydrochloric alcohol for one to two seconds, washed with running water for several minutes, stained by ponceau-acid fuchsin, and further washed with running water. Following this, the specimens were treated with phosphoric acid solution for five minutes and re-stained with aniline blue for five minutes, treated with 1% glacial acetic acid for one minute, rinsed by running water, dehydrated, and made to be transparent and sealed. The microscope (Olympus microscope with BX51 device imaging system (Shanghai Optical Technology Co., Ltd, Shanghai, China) was used for the analyzing the specimen. H&E staining was conducted in order to detect the fracture morphology and callus formation condition, and Masson's trichrome staining was performed to examine the calcified bony callus with green colouring.

Biomechanical test. Femur specimens (five from each group) were selected 42 days after model establishment, followed by the removal of the needles used for fixing the fracture. A single-axis electromagnetic type servo-testing machine (E 1 100; Instron, High Wycombe, United Kingdom) was applied for the three-point bending experiment at room temperature. Subsequently, the femur specimens were placed on the sample carrier and kept wet during the whole the experiment, with the loading speed adjusted to 5 mm per minute with 10 mm of span. The maximum load, maximum radial degrees, elastic radial degrees, and rigidity were calculated through the load-deformation curve drawn by the computer.

Immunohistochemistry. The paraffin sections that had been prepared at 14 and 42 days after the model had been created were then conventionally baked, dewaxed, and hydrated with their antigen repaired. Following this, the sections were treated with 5% hydrogen peroxide for 20 minutes and sealed by 5% normal goat serum for one hour. Rabbit anti-mouse monoclonal antibody to SMAD6 was added (1:100; Abcam Inc., Cambridge, Massachusetts) for incubation at 4°C overnight, followed by goat anti-rabbit immunoglobulin G (IgG; 1:200; Sigma–Aldrich Chemical Company, St. Louis, Missouri) at 37°C for one hour and diaminobenzidine (DAB) solution (Sigma–Aldrich Chemical Company), followed by incubation for four to five minutes at room temperature with the avoidance of light. In addition, the specimens were redyed by haematoxylin (Shanghai Bogoo Biotechnology Inc., Shanghai, China) for 2.5 minutes, conventionally dehydrated for transparency and then mounted by neutral balsam. The samples were then observed under a light microscope (Olympus microscope with BX51 device imaging system) and were photographed with brown reaction products representing antigen localization. The known positive film was regarded as the positive control and the first antibody was replaced by phosphate buffered saline (PBS), which served as the NC. The positive depth and number of positive staining was estimated in order to determine the expression intensity of SMAD6.

Reverse transcription quantitative polymerase chain reaction (RT-qPCR). RT-qPCR was conducted to detect the miR-186 level and mRNA levels of SMAD6, BMP-2, and BMP-7. The RNA extraction kit (Invitrogen) was performed to extract the total RNA of callus tissue and cell in each group. The sequences were designed by Primer premier 5 and Oligo 6 biological software (Cabit Information Technology Co., Ltd, Shanghai, China). The sequences for forward and reverse primers for RT-qPCR were designed by Shanghai Sangon Biological Engineering Technology & Services Co., Ltd. (Shanghai, China; Table I). Moreover, the RNA was reverse transcribed to complementary DNA (cDNA) in accordance to the instructions provided on the reaction conditions PrimeScript RT reagent kit (Dalian Takara Inc., Liaoning, China) with 10 μl of reverse transcription system as follows: reverse transcription reaction at 37°C conducted three times (15 minutes each) and reverse transcriptase inactivation reaction at 85°C for five seconds. The reaction solution was used to conduct fluorescent quantitative polymerase chain reaction (PCR) according to the manual of SYBR Premix Ex Taq II kit with a total reaction system of 50 μl: 25 μl of SYBR Premix Ex Taq II (2×; Takara, Dalian, Shandong, China), 2 μl of PCR forward sequences (Takara), 2 μl of PCR reverse sequences, l μl of ROX reference dye (50×, Takara), and 4 μl of DNA template (Takara, Dalian, Shandong, China). The programme of real-time reaction (Eppendorf, Hamburg, Germany) comprised predenaturation at 95°C for 15 minutes for one cycle without collection of the fluorescence signal, followed by the PCR reaction stage: a total of 40 cycles of denaturation at 95°C for ten seconds, annealing at 58°C for

Table I. The primer sequences for reverse transcription quantitative polymerase chain reaction (RT-qPCR)

Gene	Sequence
miR-186	F: 5′-CCCGATAAA GCTAGATAACC-3′
	R: 5′-CAGTGCGTGTCGTGGAGT-3′
U6	F: 5′-GGTCGG GCAGGAAAGAGG GC-3′
	R: 5′-GCTAATCTTCTCTGTATCGTTCC-3′
BMP-2	F: 5′-GATTGACTCCATTGGCCCTA-3′
	R: 5′-GGCTAGTTTCTGGGCAGTTG-3′
BMP-7	F: 5′-CAAGTGGACATCAACGGGTT-3′
	R: 5′-GCAGGAGCGCACGATCATGT-3′
SMAD6	F: 5′-GCCACTGGATCTGTCCGATT-3′
	R: 5′-CACCCGGAGCAGTGATGAG-3′
β-actin	F: 5′-GGGCACAGTGTGGGTGAC-3′
	R: 5′-CTGGCACCACACCTTCTAC-3′

miR-186, microRNA-186; F, forward; R, reverse; BMP-2, bone morphogenetic protein-2; BMP-7, bone morphogenetic protein-7; SMAD6, SMAD family member 6; β-actin, beta-actin

20 seconds, and extension at 72°C for 30 seconds with the fluorescence signal in the extension phase collected. Finally, the dissolution curve of cycles was drawn, from 65°C to 95°C, with 0.5°C per second step by step, and the fluorescence signal was collected with the increase of the temperature. Subsequently, the reaction system was placed in a real-time PCR instrument, after which the experiment was started. The U6 was considered as the internal reference of miR-186, and beta-actin (β-actin) as internal reference of SMAD6, BMP-2, and BMP-7. The levels of miR-186, SMAD6, BMP-2, and BMP-7 were quantified using the $2^{-\triangle\triangle Ct}$ method, which was repeated three times for every gene in every sample.

Western blot analysis. The Western blot analysis was performed in order to detect the protein levels of SMAD6, BMP-2, and BMP-7 in the fracture tissue. Once the fracture tissue was selected, it was added with liquid nitrogen, ground to uniformly fine powder, and added with protein lysate. Subsequently, centrifugation was carried out with the tissue specimens at 4°C for 20 minutes with 25764 g, followed by the collection of the supernatant, which was preserved separately for subsequent experiments. The protein concentration of each sample was tested in accordance with the instructions on the bicinchoninic acid (BCA) protein quantification kit (BCA1-1KT; Sigma–Aldrich Chemical Company) and adjusted by deionized water to the same quantity as the loading buffer. After the protein was cracked via water-bathing at 100°C for ten minutes, the tissues were then placed in 10% sodium dodecyl sulphate (SDS) polyacrylamide gel for electrophoresis with the following reaction conditions: 80 V for 30 minutes, 100 V for 90 minutes, and 200 mA for 120 minutes. Afterwards, the proteins were transferred from glue to nitrocellulose membrane with 0.2 μmol/l of aperture. Furthermore, the membrane was soaked with 1 × tris-buffered saline-Tween (TBST) containing 5% skimmed milk powder, gently shaken at room temperature for one hour in order to block the nonspecific binding sites. In addition, the samples were rinsed with 1 × TBST three times (five minutes per time) and the primary antibodies were added: rabbit antibody SMAD6 (1:1000, ab13727), rabbit antibody BMP-2 (1:1000, ab14933) and BMP-7 (1:1000, ab56023), and then goat antibody β-actin (1:2000, ab8226) as the internal reference, all of which were obtained from CST Danfoss Inc. (Lowell, Massachusetts). Incubation was carried out at 4°C overnight. The primary antibodies were removed, and the samples were rinsed by 1 × TBST three times (five minutes per time), and second antibodies were added: anti-goat and anti-rabbit IgG labelled by horseradish peroxidase (1:5000, ab6785; CST, Danfoss Inc.). A reaction was carried out at room temperature for one hour. Following this, the secondary antibodies were removed and the tissues were rinsed again by 1 × TBST three times (five minutes per time). Moreover, the proteins were visualized by electrogenerated chemiluminescence (ECL) reagents (Sigma–Aldrich Chemical Company). With the β-actin used as the internal reference, the protein levels were illustrated by the ratio of the grey value of the target band and the internal reference band using Image Pro-Plus 6.0 (Media Cybernetics, San Diego, California).

Statistical analysis. SPSS 21.0 statistical software (IBM, Armonk, New York) was utilized for statistical analysis. The count data were expressed by the ratio or percentage, and the chi-squared test was used for comparison between groups. Measurement data were presented with means (SD), and one-way analysis of variance (ANOVA) was used to compare the differences among groups. A p-value < 0.05 represented a statistically significant difference.

Results

Microarray analysis for regulatory miR of SMAD6. miRNAs that could potentially regulate SMAD6 were predicted using the databases microRNA.org, TargetScan, starBase, and DIANA, after which eight miRNAs with an mirSVR score (the thermodynamic stability, the lower the score, the stronger the binding stability of miRNA-mRNA) < -1 were retrieved from microRNA.org. 28 miRAs were found to show binding sites to SMAD6 in TargetScan in the conserved 8mer, 7mer, and 6mer sites and 55 miRNAs were predicted in starBase. A total of 18 miRNAs were obtained from DIANA according to the criterion of miRNA target gene (miTG) score > 0.8. These results were then compared with one another, after which only one intersection of miR-186 was found in the Venn map (Fig. 1a). Based on this finding, it was speculated that miR-186 most likely regulates SMAD6.

Luciferase reporter vector recombinant plasmid SMAD6-Wt and SMAD6-Mut inserting SMAD6 mRNA 3′-UTR were constructed in order to detect whether SMAD6 was the direct target gene of miR-186. The results found that double fluorescent reporter gene system showed luciferase signal of SMAD6-Wt-3'-UTR cotransfection in the miR-186 transfection group was

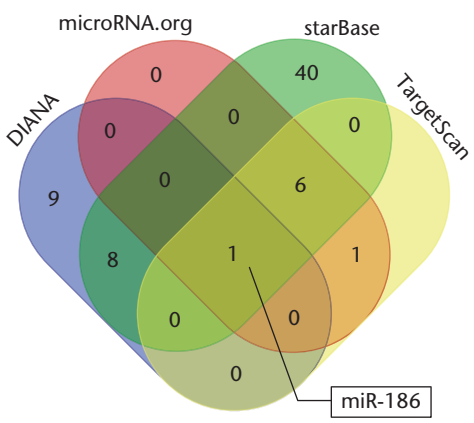

Fig. 1a

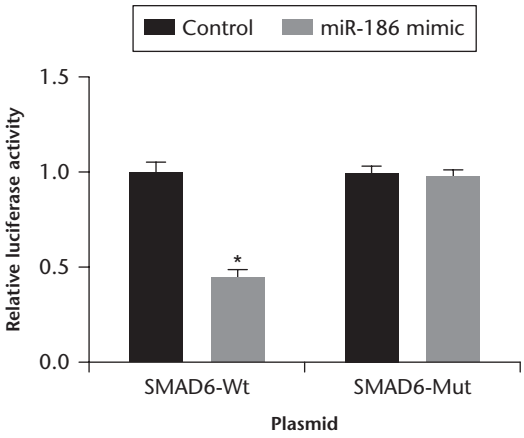

Fig. 1b

SMAD family member 6 (SMAD6) is predicted and confirmed as a target gene of microRNA-186 (miR-186). a) Only one intersection of miR-186 was found in the Venn map for prediction from four databases: microRNA.org (http://www.microrna.org/microrna/home.do), TargetScan (http://www.targetscan.org/vert_71/), starBase (http://starbase.sysu.edu.cn/index.php), and DIANA (http://diana.imis.athena-innovation.gr/DianaTools/index.php?r=microT_CDS/index); b) SMAD6 is verified as a target gene of miR-186, X-axis represents the cells were transfected with SMAD6-Wt-3'-UTR or SMAD6-mut-3'-UTR plasmid. Luciferase activities examined by dual luciferase reporter gene assay. *$p < 0.05$ *versus* the control group. Wt, wild-type; Mut, mutant.

significantly decreased in comparison with the control group (all $p < 0.05$; see Fig. 1b), while there was no significant difference in the luciferase signal of SMAD6-Mut-3'-UTR between the control and miR-186 groups (all $p > 0.05$). Thus, SMAD6 was the potential target gene of miR-186, and miR-186 could negatively target the SMAD6 mRNA levels.

Characterization of mouse models simulating femoral fracture. Next, the success rate of mouse model establishment was analyzed. The experimental mice were fixed in a dorsal position with bilateral lower limb abduction for 90° and knee flexion for 45°, after which an x-ray photography device (Faxitron MX 20 X-Ray) was used for observation. The results showed the clear skeletal morphology in normal mice (Fig. 2a) and the apparent local structure of the fracture and fracture line in the mouse models (Fig. 2b), which could be used for the assessment of the fracture state and bone healing. Out of 105 mice, 15 died and the remaining 90 were used for the subsequent experiments. All the mice were provided with normal feeding and activities within their cages. Following recovery from anaesthesia, the wound was observed to be well healed, without bleeding, swelling, or infection. The success rate of postoperative modelling was 85.71%.

Overexpression of miR-186 and silencing of SMAD6 result in significant increase in BMD and BV/TV levels. BMD (mg/cm^3) and BV/TV (%) were analyzed and calculated using 3D micro-CT. BMD was used as an indicator of bone mineral content, reflecting the degree of osteoporosis. BV/TV was an important index used for the description of the fine structure of cancellous bone, which reflected the content of BV in cancellous bone samples. After two, four, and six weeks following operation, there was an obvious increase in the levels of BMD and BV/TV in the miR-186 mimic and siRNA-SMAD6 groups when compared with the model, NC, and miR-186 inhibitor + siRNA-SMAD6 groups ($p < 0.01$), while the levels of BMD and BV/TV were decreased in the miR-186 inhibitor group ($p < 0.01$; Fig. 3). These results indicated that the overexpression of miR-186 resulted in the significant enhancement of BMD and BV/TV levels.

Overexpression of miR-186 and silencing of SMAD6 improve callus formation. H&E staining was conducted to observe the fracture morphology and callus formation condition. Trabecular bone, osteoblasts, and cartilage cells were commonly observed in the siRNA-SMAD6 and miR-186 mimic groups at two weeks. However, there was little formation of bone trabecula, few mononuclear macrophages, and many multinucleated giant cells in the model, NC, miR-186 inhibitor, and miR-186 inhibitor + siRNA-SMAD6 groups. At four weeks, the bone trabecula began interconnection with each other, osteoblasts transformed into bone cells, there was a partial merge in bone trabecula, and cartilage bone was gradually replaced by newborn bone trabecula in the siRNA-SMAD6 and miR-186 mimic groups. The formation of bone trabecula increased more than before, while little interconnection and only a small amount of bone formation was observed in the model, NC, miR-186 inhibitor, and miR-186 inhibitor + siRNA-SMAD6 groups. Furthermore, at six weeks the siRNA-SMAD6 and miR-186 mimic groups had trabecular bone remodelling, lamellar bone transformation, and a small amount of fibrous bone but more osteoclasts were observed. There was a partial merge in bone trabecula, partial cartilage bone was gradually replaced by newborn bone trabecula, and a great amount of fibrous bone was found in the model, NC, miR-186 inhibitor, and miR-186 inhibitor + siRNA-SMAD6 groups (Fig. 4).

Masson's trichrome staining was performed to observe the calcified bony callus with green colouring. Green

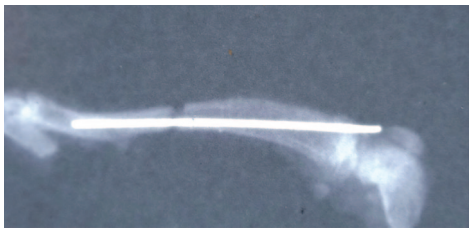

Fig. 2a

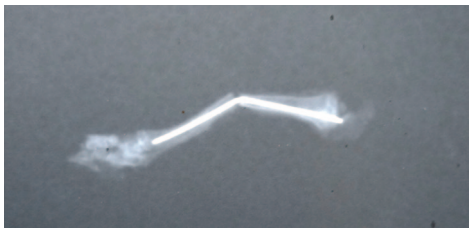

Fig. 2b

Identification of mice models of femoral fracture by x-ray scanning. a) Radiograph of the right femur of normal mice; b) radiograph of the right femur of model mice.

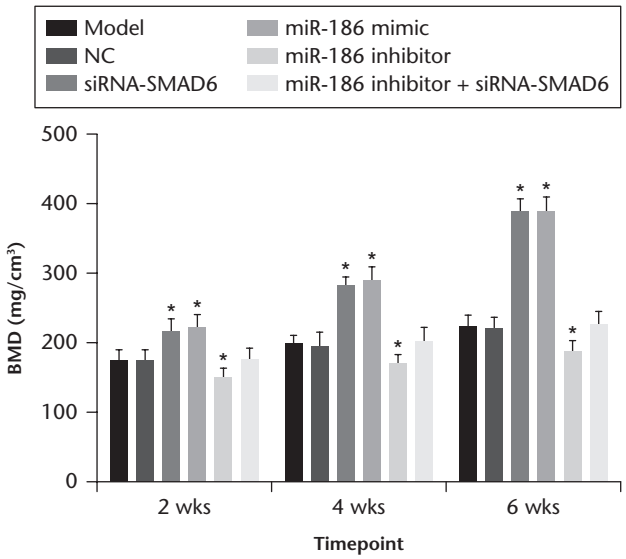

Fig. 3a

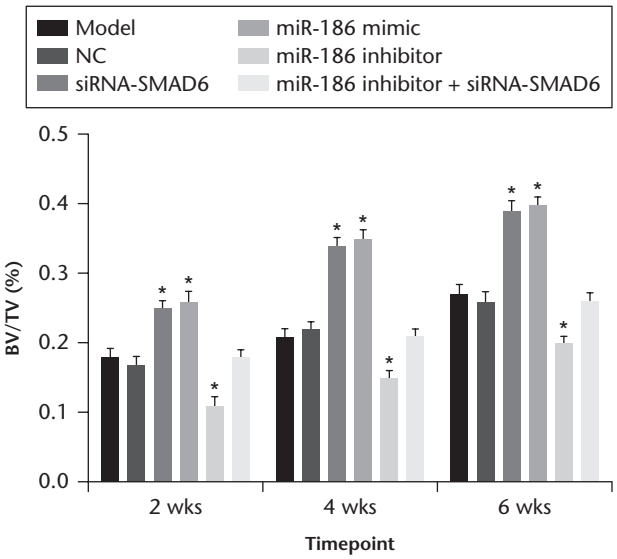

Fig. 3b

Upregulated microRNA-186 (miR-186) and inhibition of SMAD family member 6 (SMAD6) elevate bone mineral density (BMD) and bone volume fraction (BV/TV). a) BMD (mg/cm³) analyzed and calculated by 3D micro-CT; b) BV/TV (%) analyzed and calculated using 3D micro-CT. *p < 0.05 *versus* the model and negative control (NC) groups. siRNA, small interfering RNA.

staining showed the calcification of bony callus in Masson's trichrome staining. The results showed that callus was mainly composed of cartilage with little calcified bony callus. At two weeks postoperatively, the callus of the fracture end was mainly composed of cartilage and a very small amount of calcified bone and bony callus was observed in the model, NC, miR-186 inhibitor and miR-186 inhibitor + siRNA-SMAD6 groups. However, the most abundant callus formation was observed in the siRNA-SMAD6 and miR-186 mimic groups. At four weeks postoperatively, there was an increase in the calcified bone in the model, NC, miR-186 inhibitor, and miR-186 inhibitor + siRNA-SMAD6 groups, but the fracture line was blurry in the siRNA-SMAD6 and miR-186 mimic groups. At six weeks postoperatively, in each group the fracture line had disappeared and woven bone was gradually transformed into lamellar bone. However, all the groups were in the stage of callus transformation, thus the quality of cortical bone was relatively poor. Furthermore, callus reconstruction was almost complete in the siRNA-SMAD6 and miR-186 mimic groups (Fig. 5). Therefore, the findings demonstrated that there was improvement in callus formation in the presence of miR-186 overexpression and siRNA-SMAD6.

Overexpression of miR-186 and silencing of SMAD6 elevate maximum load, maximum radial degrees, elastic radial degrees, and rigidity. Biomechanical testing was performed to determine maximum load, maximum radial degrees, elastic radial degrees, and rigidity of the femur. The displacement load curve was drawn using the data of load and displacement, followed by calculation. Compared with two weeks postoperatively, the three-point bending biomechanical test results revealed that there was an increase in all the levels of maximum load, maximum radial degrees, elastic radial degrees, and rigidity in each group at four and six weeks postoperatively (all $p < 0.05$), and the levels at six weeks were higher than those at four weeks after operation. Compared with the model and NC groups, the siRNA-SMAD6 and miR-186 mimic groups presented with elevated levels of maximum load, maximum radial degrees, elastic radial degrees, and rigidity (all $p < 0.05$), while the opposite was observed in

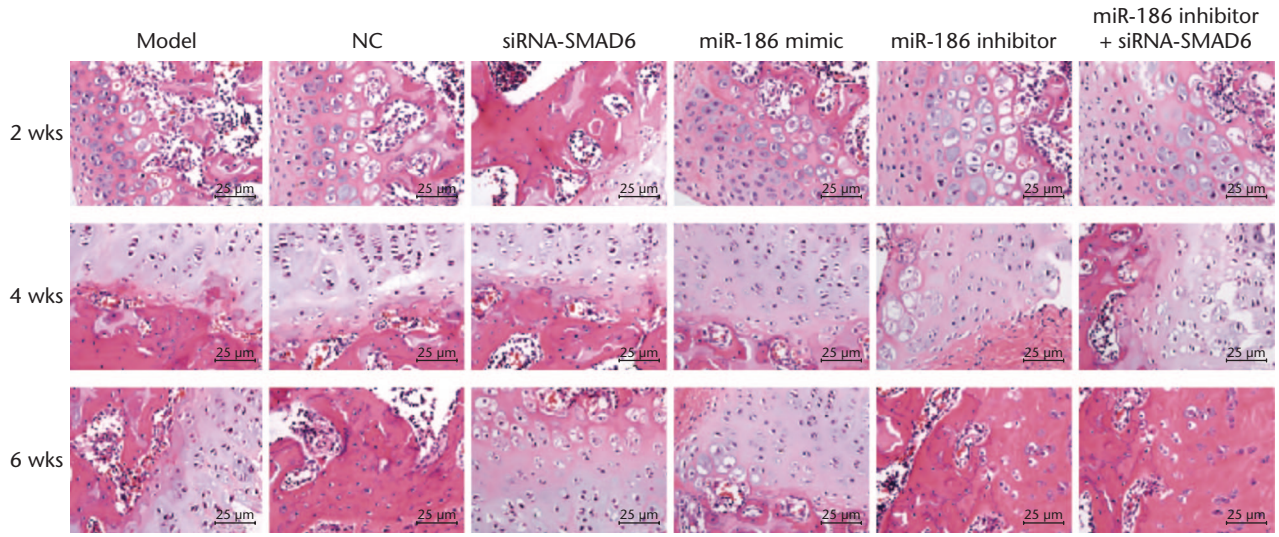

Fig. 4

Haematoxylin and eosin (H&E) staining (×400) reveals that overexpressed microRNA-186 (miR-186) and silencing SMAD family member 6 (SMAD6) led to newly formed bone trabecula. NC, negative control; siRNA, small interfering RNA.

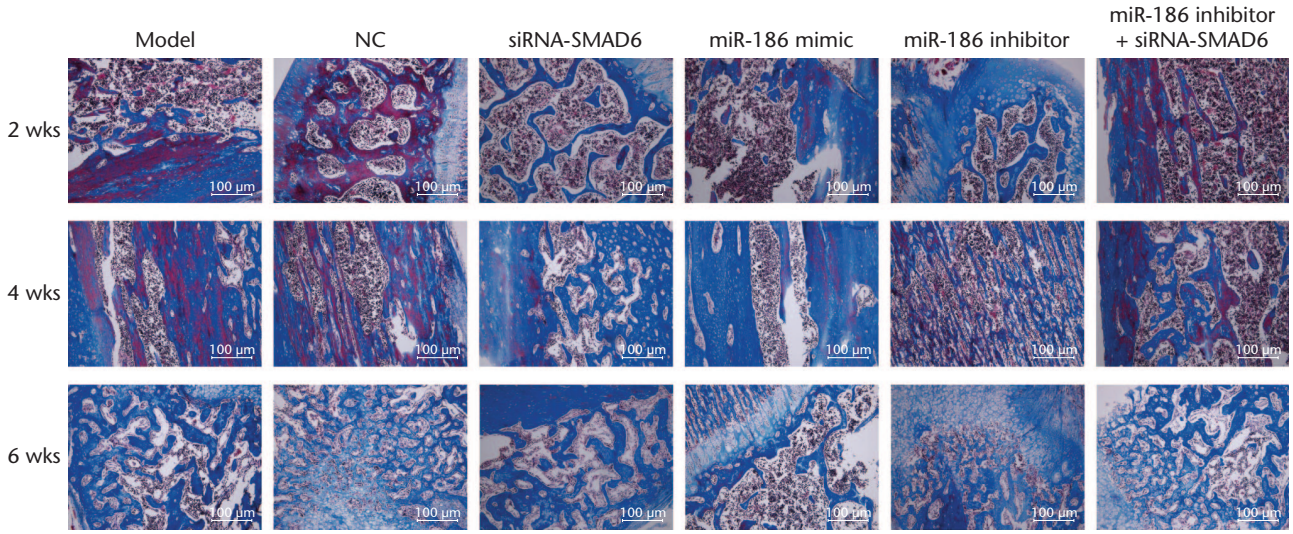

Fig. 5

Masson's trichrome staining (×100) demonstrates that overexpressed microRNA-186 (miR-186) and silencing SMAD family member 6 (SMAD6) promote callus formation. NC, negative control; siRNA, small interfering RNA; BMP, bone morphogenetic protein; β-actin, beta-actin.

the miR-186 inhibitor group (all $p < 0.05$). In addition, there was no significant difference in levels in the miR-186 inhibitor + siRNA-SMAD6 group ($p > 0.05$; Fig. 6).

Overexpression of miR-186 and silencing of SMAD6 reduce positive expression of SMAD6. Immunohistochemistry was used to detect positive expression of SMAD6 in the fracture tissue of each group and the results revealed that there was a positive expression in SMAD6 in a few osteoblasts, mature chondrocytes, fibroblasts, and bone matrix two weeks after operation in the siRNA-SMAD6 and miR-186 mimic group. The highest level in SMAD6 was observed in the model, NC, miR-186 inhibitor, and miR-186 inhibitor + siRNA-SMAD6 groups and there was a strong positive expression in osteoblasts, mature chondrocytes, fibroblasts, and bone matrix. At four and six weeks following the operation, there was a positive expression in SMAD6 in the residual osteoclasts, compared with that at four weeks (Fig. 7). The results revealed that positive expression of SMAD6 was reduced in fracture tissue in the presence of miR-186 overexpression and the silencing of SMAD6.

Overexpression of miR-186 activates the BMP signalling pathway via inhibition of SMAD6. RT-qPCR and Western blot analysis were conducted to examine miR-186 level, mRNA, and protein levels of SMAD6, BMP-2, and BMP-7 (Fig. 8). The miR-186 level, mRNA level, and protein levels of BMP-2 and BMP-7 were increased at four and six weeks following operation in comparison with those

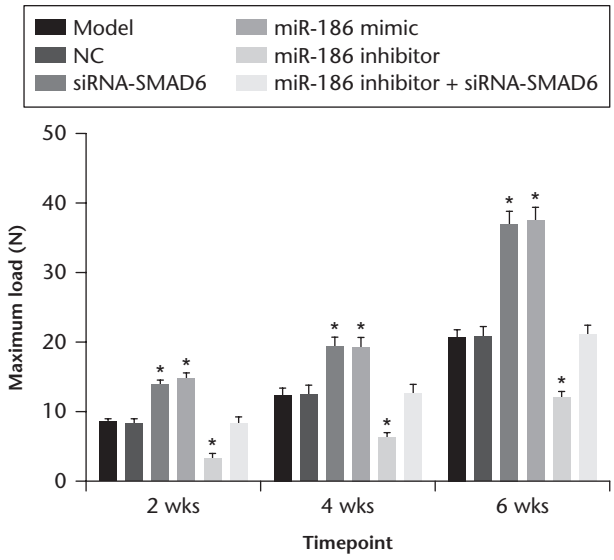

Fig. 6a

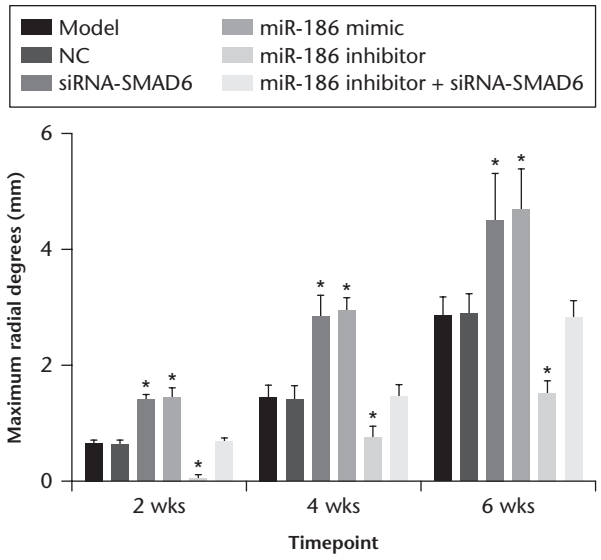

Fig. 6b

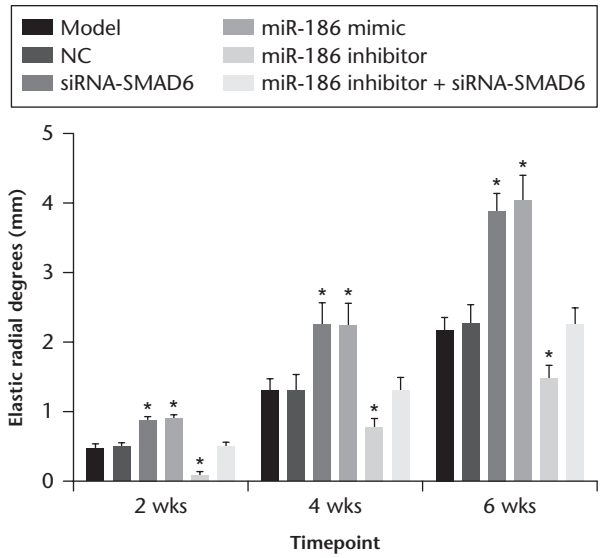

Fig. 6c

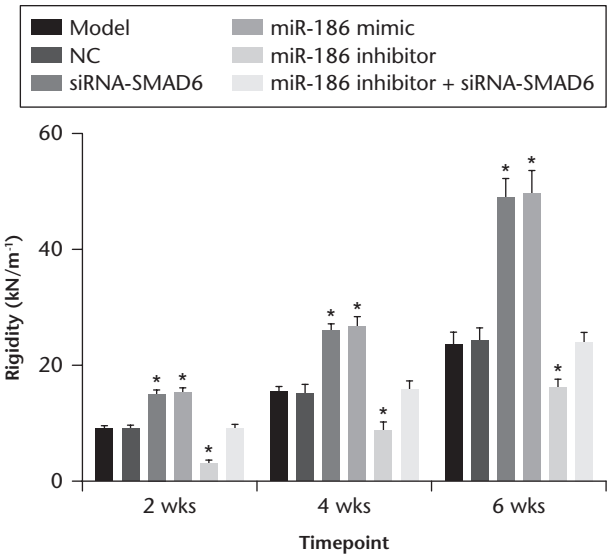

Fig. 6d

Upregulated microRNA-186 (miR-186) and silencing SMAD family member 6 (SMAD6) elevate maximum load, maximum radial degree, elastic radial degree, and rigidity. a) The maximum load of mouse femur at two, four, and six weeks after surgery; b) the maximum radial degree of mouse femur at two, four, and six weeks after surgery; c) the elastic radial degree of mouse femur at two, four, and six weeks after surgery; d) the rigidity of mouse femur at two, four, and six weeks after surgery. *p < 0.05 *versus* the model group and negative control (NC) group. siRNA, small interfering RNA.

at two weeks, but the mRNA level and protein levels of SMAD6 were decreased in each group, especially at six weeks after operation. There was no difference in mRNA level and protein levels of SMAD6 in the model and NC groups ($p > 0.05$). Compared with the model and NC groups, there was a significant decrease in the mRNA level and protein levels of SMAD6 in the miR-186 mimic group ($p < 0.05$), but increased the miR-186 level, mRNA level, and protein levels of BMP-2 and BMP-7 ($p < 0.05$). In addition, the miR-186 inhibitor group had increased the mRNA level and protein levels of SMAD6, yet decreased the miR-186 level, mRNA level, and protein levels of BMP-2 and BMP-7 ($p < 0.05$). However, there was no significant difference in the miR-186 level in the siRNA-SMAD6 group ($p > 0.05$), while there was a decrease in mRNA level, and protein levels of SMAD6 and increased mRNA level and protein levels of BMP-2 and BMP-7 ($p < 0.05$). Moreover, the miR-186 inhibitor + siRNA-SMAD6 group had decreased miR-186 level, but no significant difference was observed in other levels ($p > 0.05$).

Discussion

Bone healing is a complicated procedure dependent upon the coordinated reaction of many cell lineages in a series of biological events.[24] miRNAs have been found to

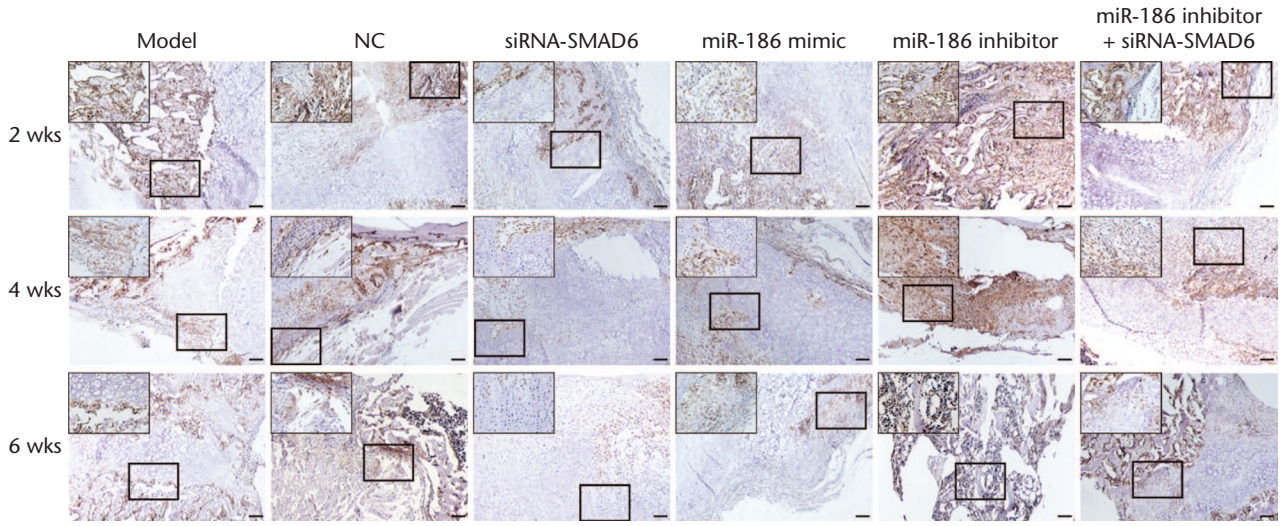

Fig. 7

Immunohistochemistry (×100) of callus tissue manifests that positive expression of SMAD family member 6 (SMAD6) is reduced by overexpressed microRNA-186b (miR-186) and silencing SMAD6. NC, negative control; siRNA, small interfering RNA.

be key regulators of the procedures necessary for tissue repair, such as inflammation, osteogenesis, angiogenesis, hypoxia response, and stem cell differentiation.[25] Therefore, the aim of this study was to elucidate the mechanisms of miR-186 on fracture healing in mice by targeting SMAD6 through mediating the bone BMP signalling pathway.

Through experiments, we have identified that overexpressed miR-186 and SMAD6 silencing resulted in markedly increased BMD and BV/TV levels. BMD is the most widely applied predictor of fracture risk.[26] Furthermore, the presence of miR-186 mimics and siRNA-SMAD6 resulted in the elevation of maximum load, maximum radial degrees, elastic radial degrees, and rigidity. miR-186 has been identified as a tumour suppressor in osteosarcoma cells by targeting PTTG1 through the suppression of the malignant phenotype and aerobic glycolysis.[27] There was an evident reduction in miR-186 in the tibia of mouse models with osteoporosis, and miR-186 mimics could impede bone deterioration by reducing cathepsin K expression in osteoclasts.[27] In addition, the dual-luciferase reporter gene assay in our study also confirmed SMAD6 as the target gene of miR-186. Wu et al[18] have shown that miR-186 targets and inhibits SMAD6, which was consistent with our results. This emphasized the finding that miR-186 and SMAD6 may be involved in the process of fracture healing. The effect of miR-186 may be through its ability of targeting and regulating SMAD6.

In addition, there was a decrease in the mRNA and protein levels of SMAD6 but BMP-2 and BMP-7 were increased in response to the treatment of miR-186 mimics. SMAD6, one of the inhibitory SMAD proteins, is required for the negative regulation of BMP and the transforming growth factor-β (TGF-β)/activin signalling; it also preferentially inhibits BMP signalling and is expressed in a cell-specific fashion.[28] BMPs, a subfamily of the TGF-β superfamily including inhibins and activins that contain 20 different proteins, have been called BMP in humans, but not all members are osteogenic.[29] The BMP-2 expression promotes fracture healing and the expression of decorin in the different parts of the nonunion area, indicating that the highest expression of BMP-2 was found in sticking scars in comparison with that of the marrow cavity contents and bone graft.[30] Blokhuis et al[31] have shown that BMP-7 could promote early diaphyseal fracture healing in mice with oestrogen deficiency. It has also been reported that the TGF-β pathway, inhibited by SMAD6, promotes the proliferation of chondrocytes but inhibits the transformation of proliferative chondrocytes into hypertrophic chondrocytes and inhibits chondrocyte maturation.[32] The depletion of TGF-β signal in the cartilage induces chondrocyte hypertrophy, which ultimately results in cartilage degeneration.[33] Pharmacological activation of the TGF-β pathway helps protect the integrity of osteoarticular cartilage in arthritis. SMAD3-deficient mice induce hypertrophy of chondrocytes, leading to osteopenia.[34] It has been reported that the overexpression of SMAD6/SMURF1 in cartilage can delay chondrocyte hypertrophy, leading to osteoporotic dwarfism.[35] The inhibition of TGF-β pathway activation by SMAD6 could suppress chondrocyte proliferation and chondrocyte hypertrophy, which leads to the impairment of bone repair. As reflected in our study, miR-186 overexpression could effectively inhibit the expressions of SMAD6 and activate the BMP signalling pathway, which was accompanied by an increase in the expression of BMP-2 and BMP-7.

Furthermore, SMAD6 is required for the BMP2-mediated suppression of myogenic genes, and this is due to the ability of the BMP signal to mediate a switch in differentiation

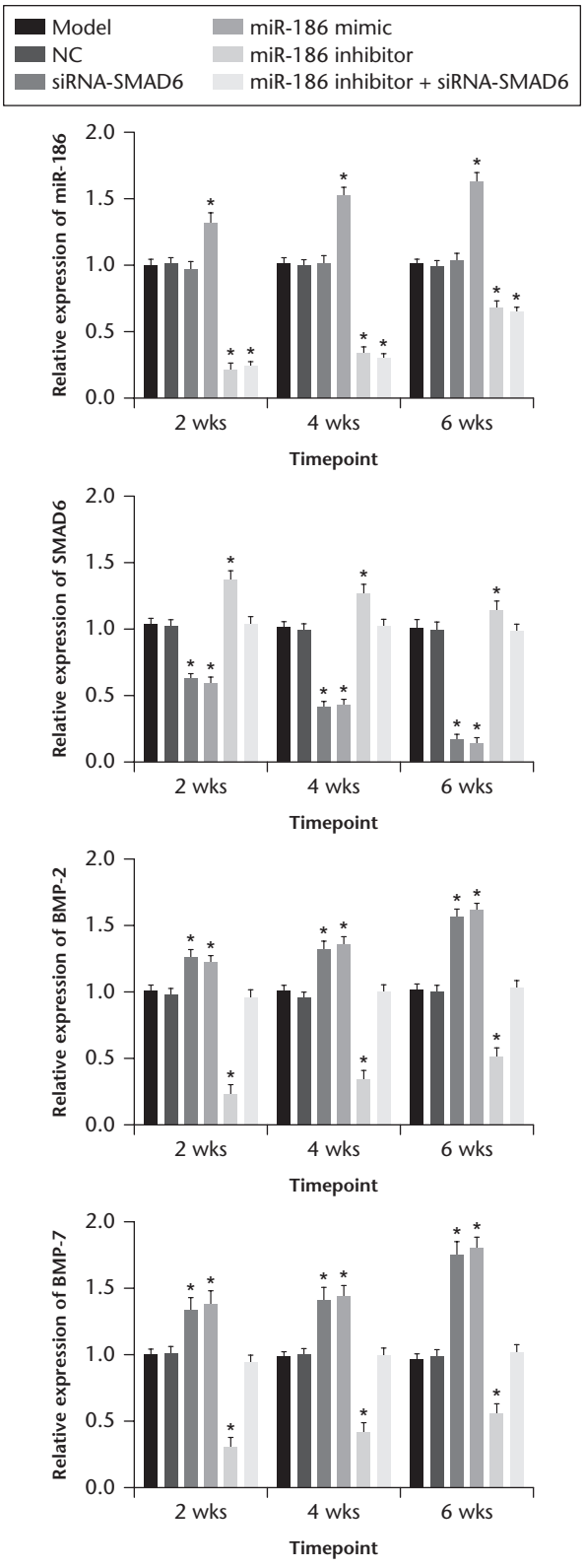

Fig. 8a

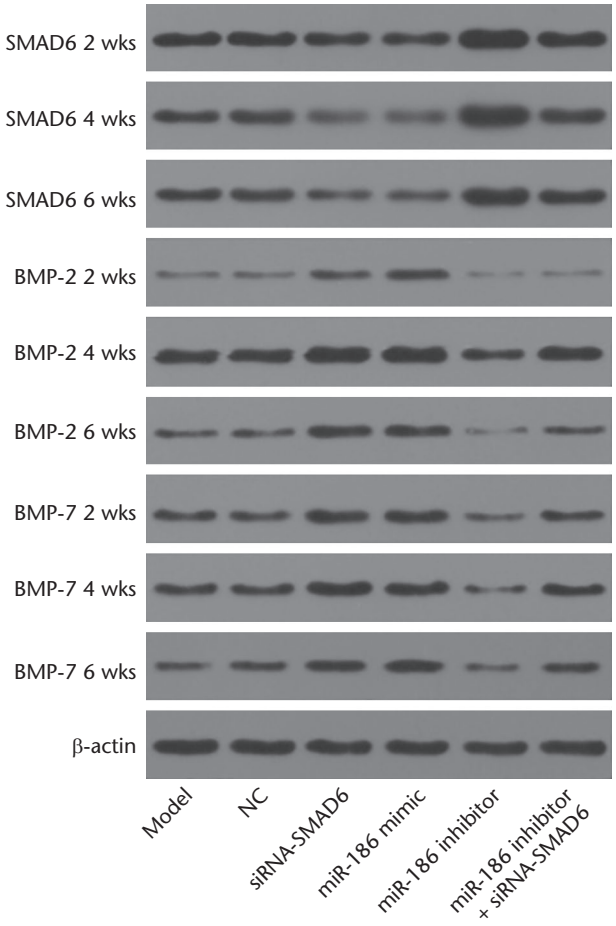

Fig. 8b

Fig. 8 (Continued)

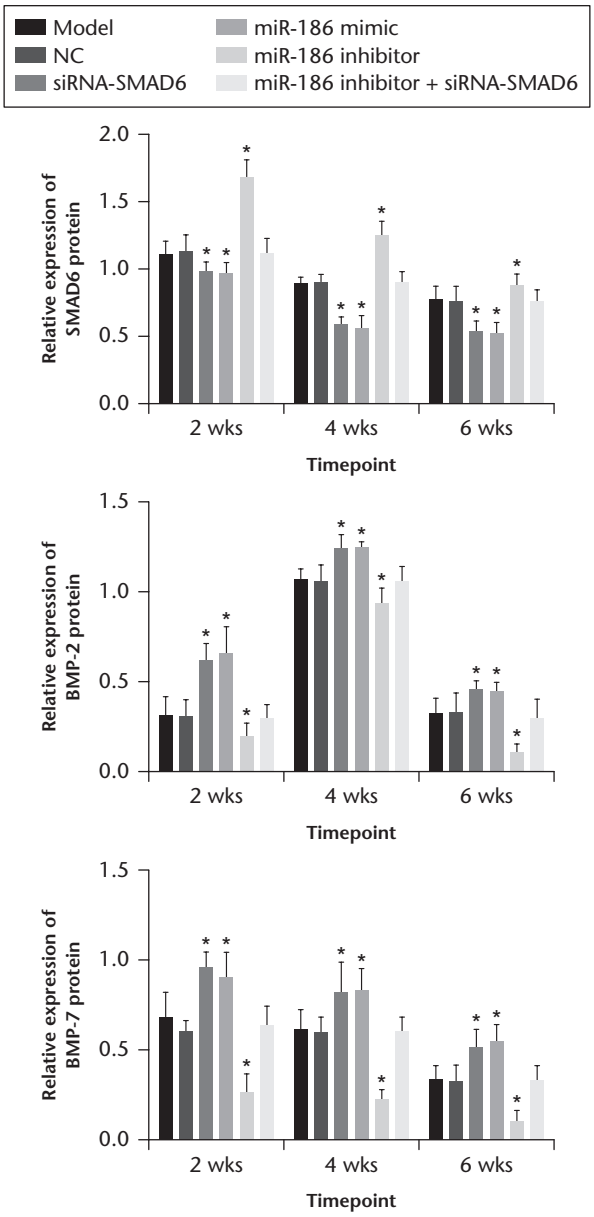

Fig. 8c

Upregulated microRNA-186 (miR-186) activates the bone morphogenetic protein (BMP) signalling pathway via inhibition of SMAD family member 6 (SMAD6). a) miR-186 level, mRNA levels of SMAD6, BMP-2, and BMP-7 after transfection detected by reverse transcription quantitative polymerase chain reaction (RT-qPCR); b) the protein bands of SMAD6, BMP-2, and BMP-7 detected by Western blot analysis; c) protein levels of SMAD6, BMP-2, and BMP-7 after transfection. *$p < 0.05$ *versus* the model group and negative control (NC) group. siRNA, small interfering RNA; β-actin, beta-actin.

of myogenic cells to the osteogenic lineage.[36] SMAD6 is required for the suppression of BMP signalling in the process of endochondral bone formation.[20] Hence a more thorough explanation of the BMP functions in bone formation and the underlying factors involved should lead to advancements in the understanding of fracture healing.[37] The BMP signalling pathway is mostly activated in fracture healing through endochondral ossification, indicating that this pathway could potentially regulate the mechanisms of healing in recruitment of skeletal progenitors.[38] Koerner et al[39] reported that fracture healing was a process in which multiple cytokines participate simultaneously. A variety of cytokines are known to determine the speed and quality of fracture healing, among which BMP is the most critical and BMP is present in the bone matrix and is the only local growth factor capable of independently inducing bone tissue formation.[40] It was reported that in the early stage of osteogenesis, BMP plays a role mainly in promoting the differentiation of stromal cells that have not yet differentiated into osteocytes, and also allows myocytes and fibroblasts to differentiate into bone cells. In the late stage of osteogenesis, it can become a differentiation factor for osteoclasts and could directly or indirectly stimulate bone cell differentiation with other factors that enhance osteoclast differentiation and participate in bone remodelling.[41] There is currently no effective means of promoting BMP secretion clinically; however, our study provides new insights in promoting BMP activation, which in turn may promote fracture healing.

In conclusion, we have shown that miR-186 can activate the BMP signalling pathway to promote fracture healing in mice by targeting SMAD6. This has indicated that miR-186 could provide a new therapeutic target in the treatment of fracture healing. Bone healing is usually composed of four distinguishable but overlapping steps, which include the early inflammatory response, soft callus formation, hard callus formation, and late bone remodelling.[42] However, our study did not identify the expression patterns of miR-186 during these three phases. Therefore, further studies are necessary to investigate the expression of miR-186 during different phases of bone healing.

References

1. **Pape HC, Marcucio R, Humphrey C, et al.** Trauma-induced inflammation and fracture healing. *J Orthop Trauma* 2010;24:522-525.
2. **Toben D, Schroeder I, El Khassawna T, et al.** Fracture healing is accelerated in the absence of the adaptive immune system. *J Bone Miner Res* 2011;26:113-124.
3. **Garrison KR, Shemilt I, Donell S, et al.** Bone morphogenetic protein (BMP) for fracture healing in adults. *Cochrane Database Syst Rev* 2010;6:CD006950.
4. **Marsell R, Einhorn TA.** The biology of fracture healing. *Injury* 2011;42:551-555.
5. **Glendenning P.** Markers of bone turnover for the prediction of fracture risk and monitoring of osteoporosis treatment: a need for international reference standards: osteoporos int 2011;22:391-420. *Clin Biochem Rev* 2011;32:45-47.
6. **Kidd LJ, Stephens AS, Kuliwaba JS, et al.** Temporal pattern of gene expression and histology of stress fracture healing. *Bone* 2010;46:369-378.
7. **Waki T, Lee SY, Niikura T, et al.** Profiling microRNA expression during fracture healing. *BMC Musculoskelet Disord* 2016;17:83.
8. **Waki T, Lee SY, Niikura T, et al.** Profiling microRNA expression in fracture nonunions: potential role of microRNAs in nonunion formation studied in a rat model. *Bone Joint J* 2015;97-B:1144-1151.
9. **Sun Y, Xu L, Huang S, et al.** mir-21 overexpressing mesenchymal stem cells accelerate fracture healing in a rat closed femur fracture model. *BioMed Res Int* 2015;2015:412327.
10. **Takahara S, Lee SY, Iwakura T, et al.** Altered expression of microRNA during fracture healing in diabetic rats. *Bone Joint Res* 2018;7:139-147.
11. **Li QS, Meng FY, Zhao YH, et al.** Inhibition of microRNA-214-5p promotes cell survival and extracellular matrix formation by targeting collagen type IV alpha 1 in

osteoblastic MC3T3-E1 cells. *Bone Joint Res* 2017;6:464-471.
12. **Lagos-Quintana M, Rauhut R, Meyer J, Borkhardt A, Tuschl T.** New microRNAs from mouse and human. *RNA* 2003;9:175-179.
13. **Chen BZ, Yu SL, Singh S, et al.** Identification of microRNAs expressed highly in pancreatic islet-like cell clusters differentiated from human embryonic stem cells. *Cell Biol Int* 2011;35:29-37.
14. **Bostjancic E, Zidar N, Glavac D.** MicroRNA microarray expression profiling in human myocardial infarction. *Dis Markers* 2009;27:255-268.
15. **Cai Z, Hao XY, Liu FX.** MicroRNA-186 serves as a tumor suppressor in oral squamous cell carcinoma by negatively regulating the protein tyrosine phosphatase SHP2 expression. *Arch Oral Biol* 2018;89:20-25.
16. **Cui G, Cui M, Li Y, et al.** MiR-186 targets ROCK1 to suppress the growth and metastasis of NSCLC cells. *Tumour Biol* 2014;35:8933-8937.
17. **Zhang ZL, Bai ZH, Wang XB, et al.** miR-186 and 326 predict the prognosis of pancreatic ductal adenocarcinoma and affect the proliferation and migration of cancer cells. *PLoS One* 2015;10:e0118814.
18. **Wu R, Shen D, Sohun H, et al.** miR-186, a serum microRNA, induces endothelial cell apoptosis by targeting SMAD6 in Kawasaki disease. *Int J Mol Med* 2018;41:1899-1908.
19. **Zhang X, Zhang J, Bauer A, et al.** Fine-tuning BMP7 signalling in adipogenesis by UBE2O/E2-230K-mediated monoubiquitination of SMAD6. *EMBO J* 2013;32:996-1007.
20. **Estrada KD, Retting KN, Chin AM, Lyons KM.** Smad6 is essential to limit BMP signaling during cartilage development. *J Bone Miner Res* 2011;26:2498-2510.
21. **Wang P, Ying J, Luo C, et al.** Osthole promotes bone fracture healing through activation of BMP signaling in chondrocytes. *Int J Biol Sci* 2017;13:996-1007.
22. **Yang B, Lin X, Tan J, et al.** Root bark of Sambucus Williamsii Hance promotes rat femoral fracture healing by the BMP-2/Runx2 signaling pathway. *J Ethnopharmacol* 2016;191:107-114.
23. **Hata A, Lagna G, Massagué J, Hemmati-Brivanlou A.** Smad6 inhibits BMP/Smad1 signaling by specifically competing with the Smad4 tumor suppressor. *Genes Dev* 1998;12:186-197.
24. **Pountos I, Georgouli T, Blokhuis TJ, Pape HC, Giannoudis PV.** Pharmacological agents and impairment of fracture healing: what is the evidence? *Injury* 2008;39:384-394.
25. **Murata K, Ito H, Yoshitomi H, et al.** Inhibition of miR-92a enhances fracture healing via promoting angiogenesis in a model of stabilized fracture in young mice. *J Bone Miner Res* 2014;29:316-326.
26. **Estrada K, Styrkarsdottir U, Evangelou E, et al.** Genome-wide meta-analysis identifies 56 bone mineral density loci and reveals 14 loci associated with risk of fracture. *Nat Genet* 2012;44:491-501.
27. **Xiao Q, Wei Z, Li Y, et al.** miR-186 functions as a tumor suppressor in osteosarcoma cells by suppressing the malignant phenotype and aerobic glycolysis. *Oncol Rep* 2018;39:2703-2710.
28. **Konrad L, Scheiber JA, Bergmann M, Eickelberg O, Hofmann R.** Identification of a new human Smad6 splice variant. *Andrologia* 2008;40:358-363.
29. **Lissenberg-Thunnissen SN, de Gorter DJ, Sier CF, Schipper IB.** Use and efficacy of bone morphogenetic proteins in fracture healing. *Int Orthop* 2011;35:1271-1280.
30. **Han XG, Wang DK, Gao F, Liu RH, Bi ZG.** Bone morphogenetic protein 2 and decorin expression in old fracture fragments and surrounding tissues. *Genet Mol Res* 2015;14:11063-11072.
31. **Blokhuis TJ, Buma P, Verdonschot N, Gotthardt M, Hendriks T.** BMP-7 stimulates early diaphyseal fracture healing in estrogen deficient rats. *J Orthop Res* 2012;30:720-725.
32. **Wu M, Chen G, Li YP.** TGF-β and BMP signaling in osteoblast, skeletal development, and bone formation, homeostasis and disease. *Bone Res* 2016;4:16009.
33. **Zhang T, Wen F, Wu Y, et al.** Cross-talk between TGF-beta/SMAD and integrin signaling pathways in regulating hypertrophy of mesenchymal stem cell chondrogenesis under deferral dynamic compression. *Biomaterials* 2015;38:72-85.
34. **Borton AJ, Frederick JP, Datto MB, Wang XF, Weinstein RS.** The loss of Smad3 results in a lower rate of bone formation and osteopenia through dysregulation of osteoblast differentiation and apoptosis. *J Bone Miner Res* 2001;16:1754-1764.
35. **Horiki M, Imamura T, Okamoto M, et al.** Smad6/Smurf1 overexpression in cartilage delays chondrocyte hypertrophy and causes dwarfism with osteopenia. *J Cell Biol* 2004;165:433-445.
36. **Chen YL, Liu B, Zhou ZN, et al.** Smad6 inhibits the transcriptional activity of Tbx6 by mediating its degradation. *J Biol Chem* 2009;284:23481-23490.
37. **Kloen P, Di Paola M, Borens O, et al.** BMP signaling components are expressed in human fracture callus. *Bone* 2003;33:362-371.
38. **Yu YY, Lieu S, Lu C, et al.** Immunolocalization of BMPs, BMP antagonists, receptors, and effectors during fracture repair. *Bone* 2010;46:841-851.
39. **Koerner JD, Markova DZ, Schroeder GD, et al.** The local cytokine and growth factor response to recombinant human bone morphogenetic protein-2 (rhBMP-2) after spinal fusion. *Spine J* 2018;18:1424-1433.
40. **Müller CW, Hildebrandt K, Gerich T, et al.** BMP-2-transduced human bone marrow stem cells enhance neo-bone formation in a rat critical-sized femur defect. *J Tissue Eng Regen Med* 2017;11:1122-1131.
41. **Nguyen HT, Ono M, Oida Y, et al.** Bone marrow cells inhibit BMP-2-induced osteoblast activity in the marrow environment. *J Bone Miner Res* 2019;34:327-332.
42. **Lu H, Zheng C, Wang Z, et al.** Effects of low-intensity pulsed ultrasound on new trabecular bone during bone-tendon junction healing in a rabbit model: a synchrotron radiation micro-CT study. *PLoS One* 2015;10:e0124724.

Author information
- C. Wang, MB, Associate Senior Doctor, MRI Department, Huadong Hospital Affiliated to Fudan University, Shanghai, China.
- G-F. Zheng, MM, Chief Physician, Department of Orthopedics, The Yuhang Hospital Affiliated to Medical College of Hangzhou Normal University, Hangzhou, China.
- X-F. Xu, MM, Associate Senior Doctor, Department of Clinical Laboratory, Fudan University Shanghai Cancer Center, Shanghai, China; Department of Oncology, Shanghai Medical College of Fudan University, Shanghai, China.

Author contributions
- C. Wang: Wrote the main manuscript text, Contributed to the revised manuscript.
- G-F. Zheng: Prepared table and figures, Contributed to the revised manuscript.
- X-F. Xu: Collected the data, Contributed to the revised manuscript.
- C. Wang and G-F. Zheng are regarded as co-first authors.

Funding statement
- No benefits in any form have been received or will be received from a commercial party related directly or indirectly to the subject of this article.

Acknowledgements
- The authors would like to give their appreciation to the reviewers for their comments on this article.

Ethical review statement
- The present study was carried out in strict accordance with the recommendations in the Guide for the Care and Use of Laboratory Animals of the National Institutes of Health. The study was conducted with the approval of our university's Institutional Animal Care and Use Committee.